Journal of Zhejiang University-SCIENCE A (Applied Physics & Engineering)
ISSN 1673-565X (Print); ISSN 1862-1775 (Online)
www.zju.edu.cn/jzus; www.springerlink.com
E-mail: jzus@zju.edu.cn

Design and experimental verification of a new multi-functional bridge seismic isolation bearing*

Chen-xi XING, Hao WANG†‡, Ai-qun LI, Ji-rong WU

(*MOE Key Laboratory of Concrete and Prestressed Concrete Structures, Southeast University, Nanjing 210096, China*)

†E-mail: wanghao1980@seu.edu.cn

Received Apr. 15, 2012; Revision accepted July 16, 2012; Crosschecked Nov. 16, 2012

Abstract: A new multi-functional bridge seismic isolation bearing (MFBSIB) is designed and its mechanical model is developed in this paper. Combining an upper sliding device and a lower energy dispassion isolation device effectively, the new MFBSIB can adjust the deformation caused by temperature, vehicle breaks, and concrete creep, etc., in addition to dissipating energy. The switch of 'slide-isolation' is achieved and the efficiency of both upper and lower parts is validated through experiment with a model. The shear performance curve established in this paper is verified to be efficient in describing the mechanical characteristics of the bearing through experiment. It is proved through both numerical calculation and experimental analysis that the new MFBSIB is endowed with enough vertical rigidity, good energy dissipation ability, stable overall performance, and good realization in expected goals. Its performance is slightly influenced by shear stress, while affected by vertical pressure, loading frequency, slide limit, etc., diversely. The results could provide reference for study and application of the new MFBSIB.

Key words: Seismic isolation bearing, Sliding device, Finite element analysis, Model experiment, Bridge
doi:10.1631/jzus.A1200106 **Document code:** A **CLC number:** U443.36

1 Introduction

Earthquakes, with an increasing frequency of occurrence in recent years, are one of the most catastrophic natural disasters in the world. With booming developments in the economy and science, China is undergoing extensive transportation infrastructure constructions. Secondary disasters caused by damages of bridges, which are always located in railway and highway traffic hubs, would bring a more serious loss of both life and property (Jangid, 2004).

Base-isolation technologies, which have been broadly developed since the appearance of layered elastomeric bearings, play an important role in the development of bridge engineering. As an effective way to control seismic response of structures, base-isolation technologies improve the structural seismic performance by adjusting their natural vibration frequency or enlarging the damping ratio. Many studies have been focused on characteristics of different bearings and seismic responses of isolated bridges, including fundamental mechanical characteristics and long-term performances of Teflon sliding bearings and lead core rubber bearings. Several Teflon dynamic tests on polytetrafluoroethylene (PTFE) sliding layers under earthquake conditions are conducted by Tyler (1977). Mathematical models for the mechanical behavior of Teflon sliding bearings in base isolation are established, and the models are validated by the testing (Constantinou *et al*., 1990). Younis and Tadjbakhsh (1984) studied the response of sliding rigid structure to base excitation including harmonic motions. As for rubber bearings, Hwang *et al*. (2002) presented a mathematical hysteretic model for

‡ Corresponding author

* Project supported by the National Natural Science Foundation of China (Nos. 50725828, 50908046, and 50978056), the Teaching & Scientific Research Fund for Excellent Young Teachers of Southeast University, the Basic Scientific & Research Fund of Southeast University (No. Seucx201106), and the Priority Academic Program Development of Jiangsu Higher Education Institutions, China

elastomeric isolation bearings, and the model is validated based on the comparison between experimental and analytical results. Tsai *et al*. (2003) conducted an extensive experimental study on identifying the mechanical characteristics of high damping rubber bearings. Pradeep Kumar and Paul (2007) studied the force-deformation behavior of lead-rubber isolation bearings. Kelly and Konstantinidis (2011) studied and summarized the mechanics of rubber bearings for seismic and vibration isolation of different structures in detail. In base-isolation technology applications, various analytical models have been proposed. For example, Nagarajaiah *et al*. (1991) presented an analytical model and a solution algorithm for nonlinear dynamic analysis of isolation system using a 3D-base-isolated structure. Kikuchi and Aiken (1997) proposed an analytical hysteresis model for elastomeric seismic isolation bearings, and the validity of the proposed model is proved by the model tests. Seismic responses of isolated bridges are also studied. For instance, Shen *et al*. (2004) studied the performance of a seismically isolated bridge under near-fault earthquake ground motions. Jangid (2004) conducted seismic response analysis on bridges seismically isolated by lead-rubber bearings (LRBs) to bidirectional earthquake excitation. Some attempts have been made to combine different isolations. Zhou *et al*. (2003) studied three failure-prevention approaches of seismic isolation rubber bearings for building structures, which introduced a backup supporter with a friction sliding plate on the top adjoin the rubber bearing. Constantinou *et al*. (1991) described a building-oriented isolation system which is a combination of a sliding bearing and helical-steel-spring. However, there is little research concerning a bridge-oriented multi-functional bearing that can obtain displacement release and energy dissipation simultaneously.

A new multi-functional bridge seismic isolation bearing (MFBSIB) orienting beam bridges is designed. Mechanical behaviors and dissipation principles are studied. Shear performance curve of the bearing is established, and shear performance correlation is studied through experiments. To validate the reliability of the bearing, the numerical results are compared with those from experimental analysis. The conclusions can provide references for the further application of the new MFBSIB.

2 Design and working principle of the multi-functional bridge seismic isolation bearing (MFBSIB)

2.1 Working principle of sliding isolation bearings

The sliding isolation bearing, which uses the relatively low coefficient of sliding friction between stainless steel and Teflon material, has come into being for more than 40 years. Its relatively large permissible horizontal displacement, which allows free transmutation between upper structure and piers, endows it with a high adaptability as movable bearings. The simplified force-displacement diagram of the sliding bearings is shown in Fig. 1 (Constantinou *et al*., 1990).

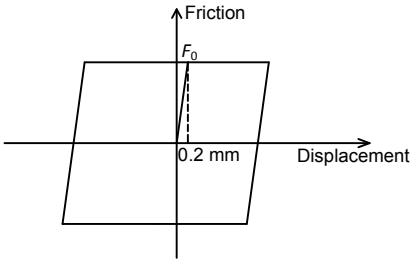

Fig. 1 Force-displacement diagram of sliding bearings (Constantinou *et al*., 1990)

Friction F can be obtained by

$$F_0=\mu_f N, \tag{1}$$

where μ_f is the coefficient of friction determined by experiment and N is the vertical pressure of the bearing.

2.2 Working principle of lead core rubber bearings

Lead core rubber bearing, which bears vertical pressure, horizontal shear and provides certain restoring force, can extend natural period of structures and dissipate energy from earthquake while its relatively high initial shear rigidity limits the deformation capacity in normal conditions. Fig. 2 shows the hysteresis curve of the bilinear restoring force model of lead core rubber isolation device, where K_i, K_d, and Q_d are initial rigidity, rigidity after yield, and yield stress, respectively; K_{eq} indicates horizontal equivalent stiffness (JG 118-2000). These are important parameters of lead core rubber bearings and can be calculated from the load-displacement hysteresis curve.

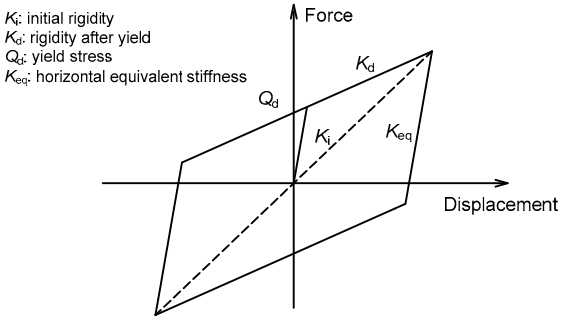

Fig. 2 Hysteresis curve of bilinear restoring force model of lead core rubber bearing

2.3 Working principle of the new multi-functional bridge seismic isolation bearing (MFBSIB)

The new MFBSIB integrates the advantages of the two bearings mentioned above and overcomes their drawbacks by combining them together (Fig. 3).

Fig. 3 shows that this new bearing combines the upper sliding device and lower lead core rubber isolation (LRI) device in series. Thus, it can protect the structure by adapting the deformation caused by temperature, vehicle breaks, and concrete creep, etc., through glide provided by the upper sliding device. Baffles are adjustable to alter slide limit, and both unidirectional and bidirectional bearings could be achieved. The procedures are as follows: the LRI device makes a tiny displacement and transfers the force to the upper sliding device at the beginning. Acting as an isolation, the upper sliding device begins to glide after the shear force of the LRI device exceeds the maximum static friction force of the sliding device. The switch device takes action and motivates the lower LRI device when the upper cover plate of LRI device hit the baffle after sliding displacement reaches the designed slide limit, and the LRI device begins to show typical bilinear hysteretic dissipation characteristics. LRI device starts to recover vertically after reaching the maximum displacement, and no slide occurs during this procedure as the restoring force is smaller than friction. The next 'slide-isolation' circulation starts after the LRI device recovers vertical.

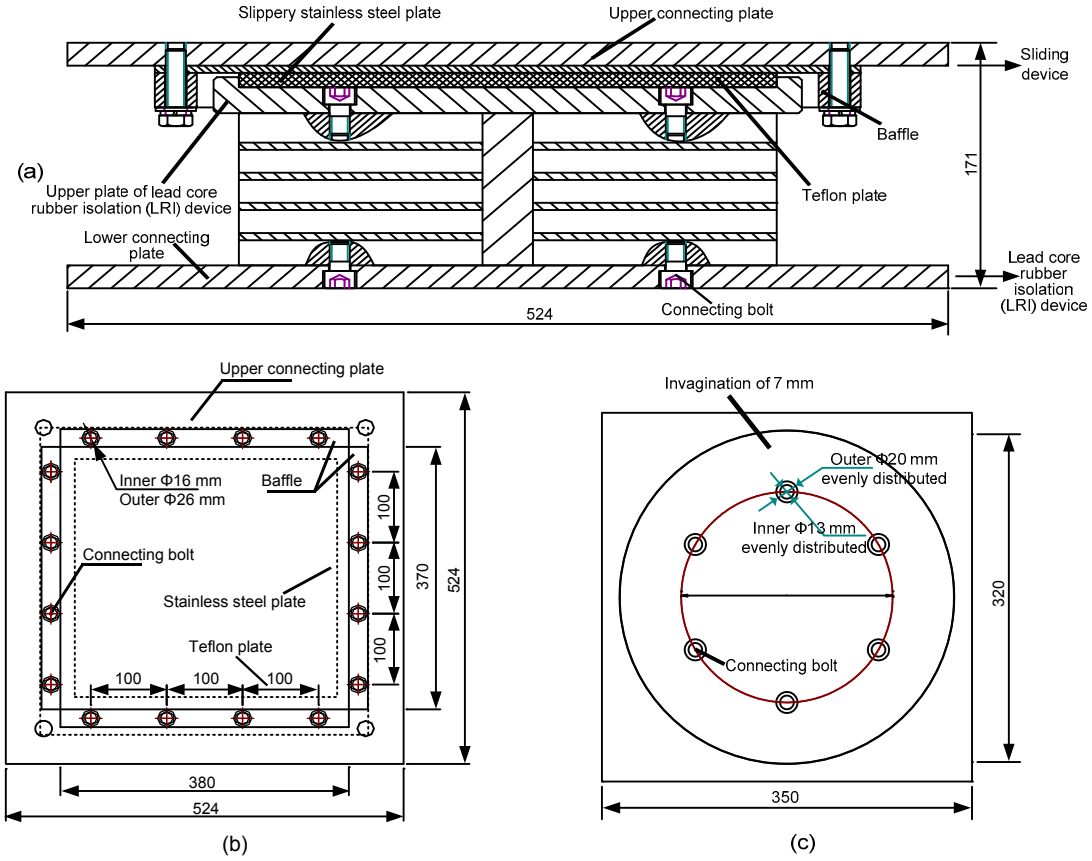

Fig. 3 Conformation and model size of multi-functional bridge seismic isolation bearing (MFBSIB) (unit: mm)
(a) Front view of the MFBSIB model; (b) Top view of sliding device; (c) Lower configuration of sliding device

3 Mechanical properties of multi-functional bridge seismic isolation bearing (MFBSIB)

3.1 Establishment of finite element model of lead core rubber isolation (LRI) device

The finite element (FE) analysis software ANSYS is applied here for simulation and analysis by setting up a solid model of the bearing. Lead core of the LRI device, rubber, sandwich plate, sealing plate are simulated by SOLID 185. Staying elasticity under stress, the sandwich plate and sealing plate, which adopt Q235 steel with Ex of 210 GPa and Poisson's ratio of 0.3, are simulated by linear elastic model. The elastomeric material, which obtains a large deformation and appears complex material nonlinearity and geometric nonlinearity, can be regarded as super elasticity and nearly incompressible material, and it is simulated by Mooney-Rivlin model in calculation. The lead core can be simplified as ideal elastoplastic material and is simulated by bilinear isotropic hardening model-BISO. The size of the lead core bearing applied is shown in Table 1. Shape factors mentioned in Table 1 are applied to calculate the expansion effect of rubber. The mechanical parameters of LRB, which are derived based on correlative theories, are shown in Table 2 (GB/T 20688.2-2006). In Table 2, the shear deformation is 100% when concerning horizontal properties of LRB.

Free partition is applied to the lead core of the LRI device and the remaining rubber and sandwich plate use cube mapping division. All degrees of freedom of the lower connection plate are restricted. Axial pressure is placed on top of the upper connecting plate. The coupling order (CP) is applied to coupling all degrees of freedom of the upper connecting plate together, and a sine wave load is placed on the coupling point.

3.2 Parameter analysis of force-displacement hysteresis curve for lead core rubber isolation (LRI) device

Four conditions are simulated as in Table 3. As shown in Fig. 4, loading frequency has no influence on hysteresis curve, and vertical pressure plays little effect on hysteresis curve within 10 MPa as curves appear quite close to each other.

3.3 Theoretical shear performance curve of the multi-functional bridge seismic isolation bearing (MFBSIB)

The combination of the working principle and the results of the FE analysis of this new bearing, force-displacement hysteresis curve of the bearing with shear strain of 100%, vertical pressure of 350 kN, slide limit of 30 mm, and friction coefficient of 0.03 is concluded in Fig. 5, in which the shear strain indicates that of LRI device only.

Table 1 Size of lead-rubber bearing (LRB) applied in ANSYS

Parameter	Value
Elastic shear modulus of rubber (MPa)	0.392
Effective diameter (mm)	300
Diameter of lead core (mm)	60
Rubber parameter (layer×thickness) (mm)	18×3.39=61
Steel plate parameter (layer×thickness) (mm)	17×1.5=25.5
Thickness of upper and lower connecting plate (mm)	10
1st shape factor (effective pressure area/ free side superficial area of each layer)	22.12
2nd shape factor (steel plate diameter/ total rubber height)	4.92
Total height (mm)	106.5

Table 2 Theoretical analysis results on mechanical properties of lead-rubber bearing (LRB)

Parameter	Value
Vertical rigidity (kN/mm)	862
Rigidity before yield (kN/m)	4569
Rigidity after yield (kN/m)	457
Yield stress (kN)	22.5
Horizontal equivalent stiffness (kN/m)	826
Equivalent damping ratio (%)	26.50

Table 3 Finite element (FE) computation conditions concerning loading frequency and vertical pressure

Condition	Vertical pressure (MPa)	Loading frequency (Hz)	Shear strain (%)
I	5	0.1	50
II	5	0.2	50
III	5	0.1	50
IV	10	0.1	50

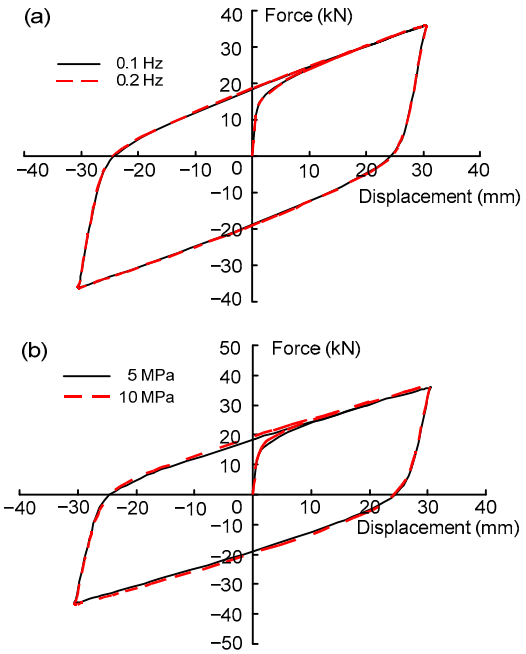

Fig. 4 Parameter analysis on load-displacement hysteresis curve of the finite element (FE) model
(a) Loading frequency; (b) Vertical pressure

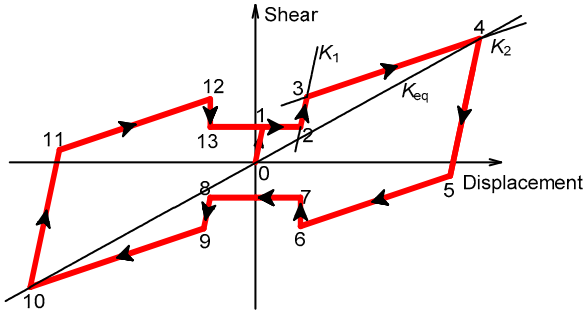

Fig. 5 Shear deformation curve by theoretical analysis

Numbers 0 to 13 are mechanical key points in the procedure of bearing deformation, and 0 is the beginning point. Procedure 0–1 denotes the force-displacement curve of the LRI device controlled by the rigidity before yield K_1. Point 1 is the starting sliding point, where the force is sliding friction. Process 1–2 indicates the sliding section, among which friction is assumed stable. From point 2, the end of sliding section, the switch device begins to motivate the lower LRI device. Procedure 2–3 reveals the force-displacement curve of the LRI device dominated by the rigidity before yield K_1. Point 3 is the yield point of the lead core. Step 3–4 expresses the force-displacement curve of the LRI device dominated by rigidity after yield K_2. After point 4, where shear deformation reaches 100%, the bearing gets shear force in the reverse direction. Procedure 4–5 represents the deformation curve after the bearing begins to restore vertical before the LRI device's reverse yielding, which is simplified to be controlled by K_1. Point 5 is the reverse yield point of the lead core. Process 5–6 illustrates the force-displacement curve of the LRI device dominated by the rigidity after yield K_2. When it comes to point 6, where the shear force equals the static friction, the upper sliding device starts to work. Step 6–7 demonstrates the partial uploading of the sliding device considering the alternation from static friction to dynamic friction. The shear force on point 7 equals dynamic friction. Procedure 7–8 shows the sliding section, where friction is assumed stable. Procedures 8–13 resemble that of procedures 2–7 as the shear performance is not influenced by direction. The next 'slide-isolation' circulation starts after point 13. Horizontal equivalent stiffness of this new MFBSIB K_{eq} is defined as slope from points 4 to 10.

4 Test on mechanical characteristics of multi-functional bridge seismic isolation bearing (MFBSIB)

4.1 Model design and loading equipment

As shown in Fig. 6, a model is built according to the size in Fig. 3. Nonlinear mechanical properties are studied under vertical pressure and shear force simultaneously. The size of the lead-core rubber bearing model is the same as Table 1. The test was carried out on a large press-shear machine (Fig. 7) in a structural laboratory in Huazhong University of Science and Technology, Wuhan, China.

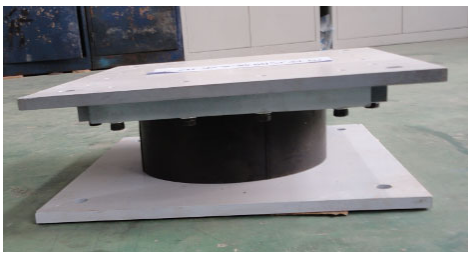

Fig. 6 Model of the multi-functional bridge seismic isolation bearing (MFBSIB)

Fig. 7 Press-shear test machine

The press-shear testing system, which consists of horizontal hydraulic servo control system, a vertical loading system, a computer system for data acquisition and analysis and control and test platform, can afford a maximum vertical pressure up to 25 MN, 2.8 MN in the horizontal direction, as well as a maximum actuation stroke of ±600 mm. The computer data acquisition and analysis system can accomplish the whole procedure of loading, data acquisition, test curve drawing, and provide the test bearing characteristic values. A sine wave is loaded horizontally and four dial indicators are settled on the corners to measure vertical displacements of bearing. The test results are reliable as the model has no damage during the whole experiment.

4.2 Vertical compression performance test

Taking 10 MPa as vertical pressure, the model is loaded three times that begins from 0 MPa to the maximum pressure and decrease to 0 MPa each time ($0 \rightarrow P_{max} \rightarrow 0$). The least effective sectional area is 70 686 mm^2. P_0 represents the design vertical pressure of 10 MPa applied on the bearing model, which equals P_0=70 686×10≈707 kN. The correlation of vertical load and vertical displacement is curved, and the third load data are analyzed and vertical rigidity K_v is calculated as follows:

$$K_v = (P_2 - P_1)/(Y_2 - Y_1), \quad (2)$$

where P_1 represents the smaller pressure in the third load, taken as $0.7P_0$; P_2 represents the larger pressure in the third load, taken as $1.3P_0$; Y_1 and Y_2 are the smaller and larger displacements in the third load, respectively. Test data are shown in Table 4. No negative phenomena like tympanic yield, bias, and asymmetric appear during the test.

Table 4 Vertical compression performance test results of the multi-functional bridge seismic isolation bearing (MFBSIB)

Parameter	Value
P_1 (kN)	495
Y_1 (mm)	0.75
P_2 (kN)	919
Y_2 (mm)	1.24
K_v (kN/mm)	865

4.3 Shear performance test

To study the mechanical properties of the new bearing comprehensively, a series of correlation tests on the shear properties are designed to examine the influence brought by different conditions. A group of tests, with the slide limit of 30 mm, vertical pressure of 350 kN and loading frequency of 0.1 Hz, are conducted at shear displacements of 30, 50, 80, 100, 120, 130, and 140 mm. Every condition is repeated three times and the test details are listed in Table 5. The conditions with slide limit of 20 mm are shown in Table 6.

Table 5 Correlation tests of shear properties with 30 mm's slip limit

Correlation item	Premise	Condition
Shear strain	350 kN, 0.1 Hz	30, 50, 80, 100, 120, 130, 140 mm
Vertical pressure	50 mm, 0.1 Hz	200, 350, 707, 848 kN
Loading frequency	50 mm, 50 kN	0.01, 0.02, 0.1, 0.2 Hz
Low pressure	200 kN, 0.1 Hz	50, 100 mm
Repeated loading	50 mm, 0.1 Hz, 200 kN	Repeat 30 times

Table 6 Correlation tests of shear properties with 20 mm's slip limit

Correlation item	Premise	Condition
Shear strain	200 kN, 0.1 Hz	50, 60, 80, 100 mm
Vertical pressure	50 mm, 0.1 Hz	200, 350 kN

4.3.1 Test results with slide limit of 30 mm

The force-displacement hysteresis curve of seven conditions with slide limit of 30 mm, vertical pressure of 350 kN, and loading frequency of 0.1 Hz is shown in Fig. 8. It can be concluded from the figure that both sliding and isolation dissipation is achieved:

friction meets no severe fluctuations and switch device functions well. Energy dissipation is well achieved by the LRO device beneath. Hysteresis curve tends to be stable from the second circle. The results of those with 20 mm slide limit are similar.

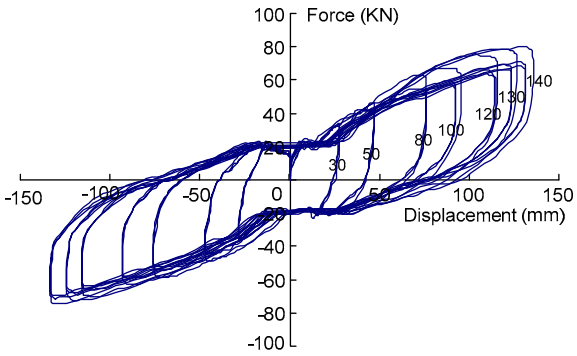

Fig. 8 Hysteresis curve on shear performance with 30 mm's slip limit

Sliding friction and starting position are acquired in both directions. Coefficient of friction is calculated to be 0.055 to 0.060. The increase of friction with growing shear strain is relatively small.

4.3.2 Shear strain correlation

The force-displacement hysteresis curve of different shear strains with slide limit of 30 mm, vertical pressure of 350 kN, and loading frequency of 0.1 Hz is shown in Fig. 9. It can be known by comparing the 3rd circle of force-displacement hysteresis curve under every condition that: energy dissipation ability rises with the growing shear strain. The function of sliding device is not much affected by shear strain, and the degenerate of LRI device is slight.

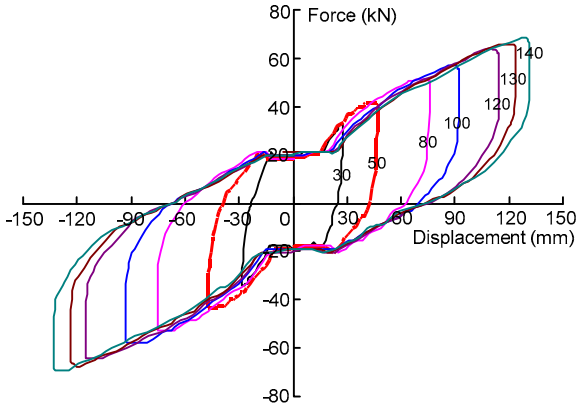

Fig. 9 Hysteresis curve on shear strain (30, 50, 80, 100, 120, 130, and 140 mm) correlation with 30 mm's slip limit

Comparison of the hysteresis curve area and equivalent horizontal stiffness denotes that equivalent horizontal stiffness of the model decreases when shear strain aggrandizes and becomes gentle after shear displacement reaches 80 mm. Equivalent damping ratio at different shear displacements are calculated in Table 7. The results indicate that the ratio diminishes as shear displacement rises and remains larger than 20%, which reveals a good ability in energy dissipation.

Table 7 Equivalent damping ratio at different shear displacements with 30 mm's slip limit

Shear displacement (mm)	Equivalent damping ratio (%)
30	30.3
50	28.5
80	25.6
100	22.5
120	21.5
130	20.9
140	21.0

4.3.3 Vertical pressure correlation

The comparison of the 3rd circle of hysteresis curve with shear displacement of 50 mm, loading frequency of 0.1 Hz under different vertical pressures (200, 350, 707, and 848 kN) is shown in Fig. 10. Ryan *et al*. (2004) studied particular effects of axial load on the bearing response and concluded that the lateral post-yield stiffness of LRBs decreases with increasing axial load and lateral yield strength decreases with decreasing axial load, which mainly correspond with Fig. 10 if the rubber bearing part is taken into consideration. The figure illustrates that vertical pressure has a relatively huge effect on the hysteresis curve of the bearing: its working principle reaches a good agreement with former theory when vertical pressures are 200 and 350 kN, though the starting position of slide differs a lot. The deformation character varies from 'slide-isolation' to 'isolation-slide' under a pressure of 707 kN. The starting point moves to 'deformation state' from 'vertical state' of LRI device as the upper friction is larger than the lower shear force but still smaller than the shear limit. When friction exceeds the shear limit with a vertical pressure of 848 kN, the switch device loses functionality and the hysteresis curve can only characterize shear performance of LRI device. As the isolation device and

sliding device were simulated separately in the FE model, the transform from 'isolation-slide' to 'pure isolation' has not been simulated numerically.

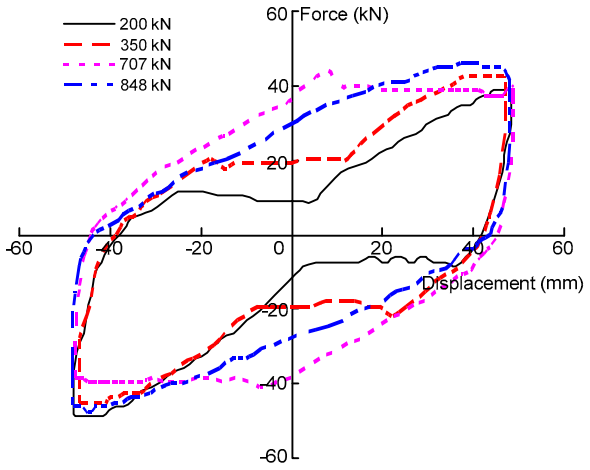

Fig. 10 Hysteresis curve on vertical pressure correlation with 30 mm's slip limit

Comparison of hysteresis curve shows that energy dissipation ability increases with a growing vertical pressure when the sliding device is still working and it reduces after switch device loses functionality.

4.3.4 Loading frequency correlation

The comparison of the 3rd circle of hysteresis curve with shear displacement of 50 mm, vertical pressure of 350 kN, loading frequencies of 0.01, 0.02, 0.1, and 0.2 Hz is shown in Fig. 11. It reveals that sliding sections are nearly consistent with similar frequencies, while the starting point of the higher frequency delays in both directions with a large gap.

The calculated enclosed areas of the hysteresis loops under excitation with different frequencies should be almost the same (Fig. 4). However, Fig. 11 shows the dissipation ability is lower with lower frequencies (0.01, 0.02 Hz). It is possibly relative to the control system of the press-shear test machine. Dissipation capacity keeps stable but does not fit a linear increase when the frequency grows and it jumps to another plateau when the frequency reaches another bound, as does the coefficient of friction. However, the uploading of the sliding device is not as distinctive as frequency grows. Thus, loading frequency has an impact on the coefficient of friction as well as the dissipation capacity.

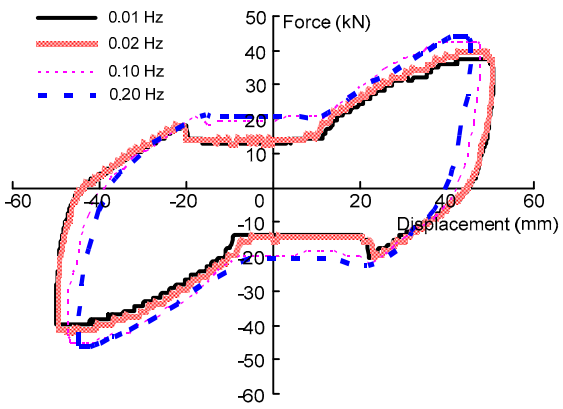

Fig. 11 Hysteresis curve on loading frequency correlation with 30 mm's slip limit

4.3.5 Low pressure correlation

Low pressure correlation provides reference to conditions with low vertical pressure but relatively high shear force of a bearing. Fig. 12 shows a good realization of 'slide-isolation' function of the model under low vertical pressure of 200 kN, loading frequency of 0.01 Hz, and shear displacements of 50 mm and 100 mm. Comparison indicates that the coefficient of friction is not influenced by the shear displacement. Sliding section in the positive direction is not affected, while it increases with enlarged shear displacement in the reverse direction, and it still accomplishes the whole slide procedure at one time. When compared with Fig. 9, the coefficient of friction decreases by 12% when the pressure increases from 200 to 350 kN. The coefficient in the reverse direction is 35% less than that of the positive direction, which explains the early appearance of the starting point. The sliding section is not only influenced by pressure, but also by the shear displacement with low pressure.

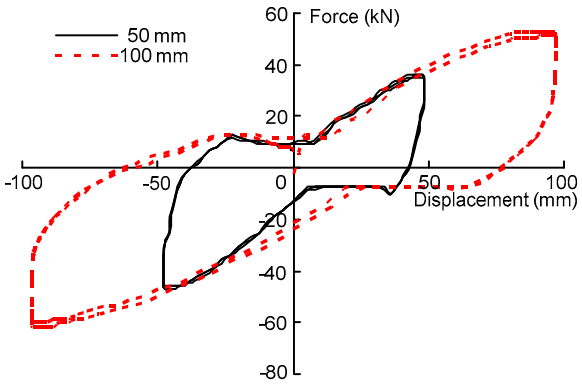

Fig. 12 Hysteresis curve on low pressure correlation with 30 mm's slip limit

4.3.6 Repeated loading correlation

Fig. 13 shows the force-displacement hysteresis curve on repeated loading (30 times), correlation with shear displacement of 50 mm, vertical pressure of 200 kN and loading frequency of 0.1 Hz. It shows the bearing has a stable dynamic hysteresis property and reliable shear performance, with small diverse in dissipation capacity, slide section and deformation characteristics under repeated loading.

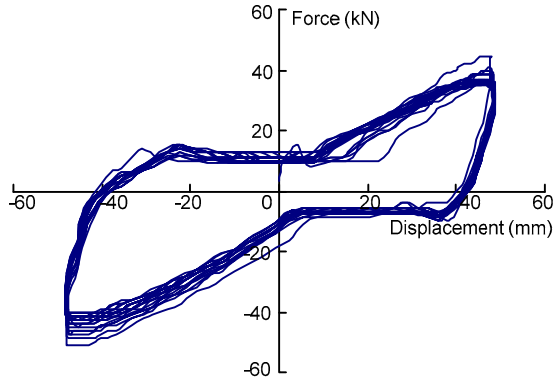

Fig. 13 Hysteresis curve on repeated loading correlation with 30 mm's slide limit

The hysteresis curve areas of circles 3, 6, 9, 12, 15, 18, 21, 24, 27, and 30 are calculated from Fig. 13. The biggest deviation of the curve area is less than 3% compared with the average, and 6% for friction which is determined by the last circle. Overall, the function of 'slide-isolation' keeps stable. The model also shows good self-centering capability during repeating loads.

4.3.7 Slide limit correlation

Three conditions are calculated to explore the effects of slide limits in Table 8.

Table 8 Conditions concerning different slide limits on shear performance

Condition	Shear displacement (mm)	Loading frequency (Hz)	Vertical pressure (kN)	Slide limit (mm)
I	50	0.1	350	20, 30
II	50	0.1	200	20, 30
III	100	0.1	200	20, 30

As shown in Fig. 14a, the starting point of the 20 mm's slide limit drops behind that of 30 mm, while their terminals are similar. The diversity of the coefficient of friction brings a difference between the two slide limits. The heaves in the hysteresis curve reflects uploading of the sliding device as analyzed above, which is because the coefficient of static friction is 10% larger than that of kinetic friction. However, this does not exist from slide to isolation. Figs. 14b and 14c illustrates that smaller pressure brings starting points closer and slide section tends to an accord with larger shear displacement. In conclusion, the effects slide limits have mainly lie on slide sections, diminishing with smaller vertical pressure and greater shear displacement.

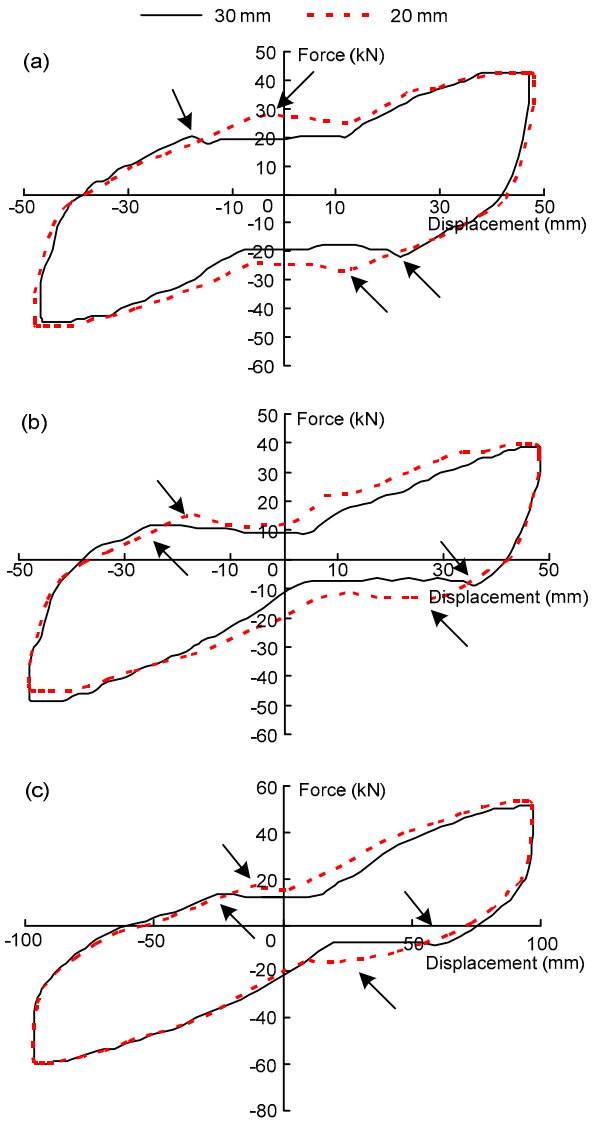

Fig. 14 Influence of spit limit on shear performance
(a)–(c) are conditions I–III in Table 8, respectively

5 Comparison of theory and experimental results

To validate the reliability of the shear deformation curve by theoretical analysis, shear performance of four conditions with theoretical and test results are compared in Table 9 to judge if the new bearing has achieved the expected goal. Shear performance curves of conditions illustrated in Table 9 are calculated based on Fig. 5 and comparable results are shown in Fig. 15. Results from tests matches well with that from theoretical analysis in both sliding and isolation periods. The loops of the LRI device appear to have high consistencies. It is less accordingly at the end of a sliding period as the rigidity after the rubber yields in test is greater than that in the theoretical analysis.

Figs. 15a and 15b reveal a better identity and symmetry with greater shear displacement. Figs. 15a and 15c show a little relevancy between slide limit and consistency. Figs. 15b and 15d indicate asymmetry of the slide section in two directions with less vertical pressure, and the partial uploading is not as significant as theory. In addition, higher loading frequency brings limited uploading periods based on Fig. 11. Overall, the shear performance curve of the new MFBSIB established in this paper can depict the mechanical properties quite well.

6 Conclusions

1. A new multi-functional bridge seismic isolation bearing (MFBSIB) is designed in this paper, its FE model is found and mechanical performance curves of the lead core isolation device are obtained in diverse conditions. Results show that the MFBSIB can not only adjust the deformation caused by temperature, vehicle breaks, and concrete creep, but can also dissipate energy. In addition, the FE analysis results indicate relatively little effects by changing the loading frequency and the vertical pressure.

Table 9 Comparative conditions of theoretical analysis and test on shear performance

Condition	Shear displacement (mm)	Loading frequency (Hz)	Vertical pressure (kN)	Slide limit (mm)
I	50	0.1	350	30
II	100	0.1	350	30
III	50	0.1	350	20
IV	100	0.1	200	30

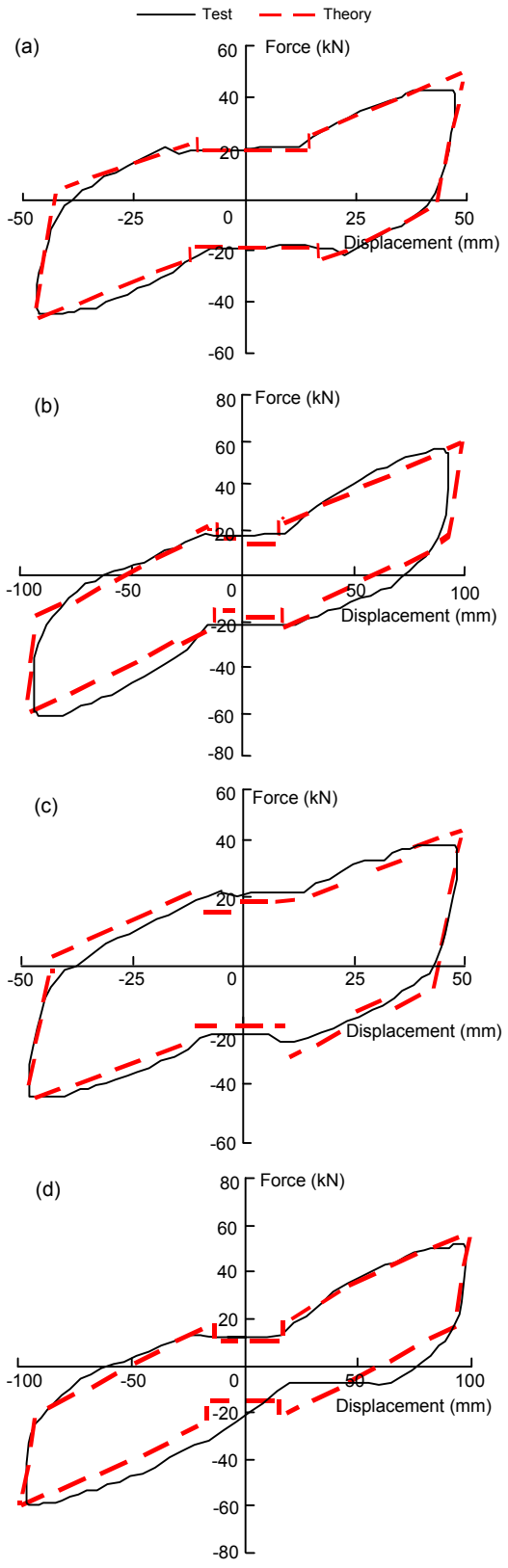

Fig. 15 Comparison on shear performance of MFBSIB
(a)–(d) show conditions I–IV in Table 9, respectively

2. Vertical compression performance test and shear performance test are launched on a model. The results illustrate that the upper sliding device, lower isolation device, and the 'slide-isolation' switch device all function well. The designed functions of friction sliding and isolation energy dissipation are achieved. The new bearing allows enough vertical rigidity. The realization of 'slide-isolation' is not seriously affected by shear strain. With increasing shear strain, the hysteresis curve area grows and equivalent stiffness decreases. The equivalent damping ratio of the model keeps larger than 20%, which reveals a good ability in energy dissipation.

3. The shear performance correlation test is launched and the results demonstrate that vertical pressure casts a huge impact on sliding sections and friction. Loading frequency influences the coefficient of friction of the upper sliding device a lot. The bearing maintains stability under repeated loading. Slide limit holds important implications for sliding sections of upper device, while the sliding sections tend to reach a consistency as vertical pressure diminishes and shear strain rises.

4. The shear performance curve of the MFBSIB established in this paper matches well with results of experiments, indicating that the shear performance curve can describe its mechanical characteristics properly, and the developed new bearing can achieve the intended goal. Therefore, the corresponding results can provide a reference for further application of bridge seismic isolation bearings.

References

Constantinou, M., Mokha, A., Reinhorn, A., 1990. Teflon bearings in base isolation II: modeling. *Journal of Structural Engineering*, **116**(2):455-474. [doi:10.1061/(ASCE)0733-9445(1990)116:2(455)]

Constantinou, M., Mokha, A., Reinhorn, A., 1991. Study of sliding bearing and helical-steel-spring isolation system. *Journal of Structural Engineering*, **117**(4):1257-1275. [doi:10.1061/(ASCE)0733-9445(1991)117:4(1257)]

GB/T 20688.2-2006. Rubber Bearing-Part II: Isolation Bearing for Bridges. China Standards Press, China (in Chinese).

Hwang, J.S., Wu, J.D., Pan, T.C., Yang, G., 2002. A mathematical hysteretic model for elastomeric isolation bearings. *Earthquake Engineering & Structural Dynamics*, **31**(4):771-789. [doi:10.1002/eqe.120]

Jangid, R.S., 2004. Seismic response of isolated bridges. *Journal of Bridge Engineering*, **9**(2):156-166. [doi:10.1061/(ASCE)1084-0702(2004)9:2(156)]

Kelly, J.M., Konstantinidis, D., 2011. Mechanics of Rubber Bearings for Seismic and Vibration Isolation. John Wiley & Sons, USA.

JG 118-2000. Rubber Isolation Bearings for Buildings. China Architecture Industry Press, China (in Chinese).

Kikuchi, M., Aiken, I.D., 1997. An analytical hysteresis model for elastomeric seismic isolation bearings. *Earthquake Engineering & Structural Dynamics*, **26**(2):215-231. [doi:10.1002/(SICI)1096-9845(199702)26:2<215::AID-EQE640>3.0.CO;2-9]

Nagarajaiah, S., Reinhorn, A.M., Constantinou, M.C., 1991. Nonlinear dynamic analysis of 3-D-base-isolated structures. *Journal of Structural Engineering*, **117**(7):2035-2054. [doi:10.1061/(ASCE)0733-9445(1991)117:7(2035)]

Pradeep Kumar, T.V., Paul, D.K., 2007. Force-deformation behavior of isolation bearings. *Journal of Bridge Engineering*, **12**(4):527-529. [doi:10.1061/(ASCE)1084-0702(2007)12:4(527)]

Ryan, K.L., Kelly, J.M., Chopra, A.K., 2004. Experimental Observation of Axial Load Effects in Isolation Bearings. 13th World Conference on Earthquake Engineering, Canada, Paper No. 1707.

Shen, J., Tsai, M.H., Chang, K.C., Lee, G.C., 2004. Performance of a seismically isolated bridge under near-fault earthquake ground motions. *Journal of Structural Engineering*, **130**(6):861-868. [doi:10.1061/(ASCE)0733-9445(2004)130:6(861)]

Tsai, C.S., Chiang, T.C., Chen, B.J., Lin, S.B., 2003. An advanced analytical model for high damping rubber bearings. *Earthquake Engineering & Structural Dynamics*, **32**(9):1373-1387. [doi:10.1002/eqe.278]

Tyler, R.G., 1977. Teflon dynamic test on PTFE sliding layers under earthquake conditions. *Bulletin of New Zealand National Society for Earthquake Engineering*, **10**(3):129-138.

Younis, C., Tadjbakhsh, I., 1984. Response of sliding rigid structure to base excitation. *Journal of Engineering Mechanics*, **110**(3):417-432. [doi:10.1061/(ASCE)0733-9399(1984)110:3(417)]

Zhou, X.Y., Han, M., Yang, L., 2003. Study on protection measures for seismic isolation rubber bearings. *ISET Journal of Earthquake Technology*, **40**(2-4):137-160.